NATIONAL UNIVERSITY OF SCIENCE AND TECHNOLOGY
POLITEHNICA BUCHAREST
(UNSTPB)

Doctoral School of
Engineering and Applications of Lasers and Accelerators

Decision No. ____ from ____-____-____

Ph.D. THESIS SUMMARY

MASS-LIMITED TARGETS FOR HIGH-POWER LASER EXPERIMENTS

ȚINTE DE MASĂ LIMITATĂ PENTRU EXPERIMENTE CU LASERI DE MARE PUTERE

Ph.D. Student: Laurențiu-Christian Dincă

THESIS COMMITTEE

CS1 Dr. habil. **Călin Alexandru UR**	President	IFIN-HH / ELI-NP
CS1 Dr. habil. **Dimiter Loukanov BALABANSKI**	Ph.D. Supervisor	IFIN-HH / ELI-NP
CS1 Dr. habil. **Daniel URSESCU**	Referee	IFIN-HH / ELI-NP
Prof. Univ. Dr. habil. **Ionuţ Cristian TOPALĂ**	Referee	”Alexandru Ioan Cuza” University of Iași / Faculty of Physics
Conf. Univ. Dr. habil. **Cătălin Nicolae MARIN**	Referee	West University of Timișoara / Faculty of Physics

BUCHAREST
2024

Acknowledgements

CS2 Dr. ***Bogdan Diaconescu*** • IFIN-HH / ELI-NP, *Măgurele* (*Ilfov*)
Ph.D. student ***Cosmin Jalbă*** • UNSTPB / SDIALA, IFIN-HH / ELI-NP, *Măgurele* (*Ilfov*)
CS1 Dr. ***Bogdana Mitu*** • INFLPR / PPMS Group, *Măgurele* (*Ilfov*)
CS3 Dr. ***Veronica Sătulu*** • INFLPR / PPMS Group, *Măgurele* (*Ilfov*)
CS3 Dr. ***Cristina Gheorghiu*** • IFIN-HH / ELI-NP, *Măgurele* (*Ilfov*)
CS3 Dr. ***Valentina Mărăscu*** • INFLPR / PPMS Group, *Măgurele* (*Ilfov*)
CS2 Dr. ***Victor Leca*** • IFIN-HH / ELI-NP, *Măgurele* (*Ilfov*)
Ph.D. student ***Alexandru Măgureanu*** • IFIN-HH / ELI-NP, *Măgurele* (*Ilfov*)
Dr. Eng. ***Mihail Cernăianu*** • IFIN-HH / ELI-NP, *Măgurele* (*Ilfov*)
CS2 Dr. ***Nikolay Djourelov*** • IFIN-HH / ELI-NP, *Măgurele* (*Ilfov*)
Technician ***Daniel Popa*** • IFIN-HH / ELI-NP, *Măgurele* (*Ilfov*)

Team of PPMS Group • INFLPR, *Măgurele* (*Ilfov*)
Teams of LDED **and** LSD • IFIN-HH / ELI-NP, *Măgurele* (*Ilfov*)

Affiliation acronyms or abbreviations:

IFIN-HH – *"Horia Hulubei" National Institute for R&D in Physics and Nuclear Engineering*
ELI-NP, within IFIN-HH – *Extreme Light Infrastructure - Nuclear Physics*
TL, within ELI-NP – *Targets Laboratory*
LDED, within ELI-NP – *Laser Driven Experiments Department*
LSD, within ELI-NP – *Lasers System Department*

INFLPR – *National Institute for Laser, Plasma and Radiation Physics*
PPMS Group, within INFLPR – *Plasma Processes, Materials and Surfaces Group*

UNSTPB – *National University of Science and Technology "Politehnica Bucharest"*
SDIALA, within UNSTPB – *Doctoral School of Engineering and Applications of Lasers and Accelerators*

Content

Keywords

Laser-driven acceleration; Thin film targets; Freestanding films;
Roughness characterization; Diamond-like carbon; Patterned substrate-corrosion;
Ultraviolet lithography

List of abbreviations

HPL – High-Power Laser
TNSA – Target Normal Sheath Acceleration
RPA – Radiation Pressure Acceleration
RIT – Relativistic Induced Transparency
BOA – Breakout Afterburner
DLC – Diamond-Like Carbon
CVD – Chemical Vapor Deposition
PECVD – Plasma Enhanced Chemical Vapor Deposition
AFM – Atomic Force Microscopy
XPS – X-Ray Photoelectron Spectroscopy
EDX – Energy Dispersive X-Ray
UV – Ultraviolet
RF – Radiofrequency
MW – Microwave
RMS – Root Mean Square
STD – Standard Deviation
3D – Three-Dimensional
2D – Two-Dimensional
IPA – Isopropanol
PMMA – Polymethylmethacrylate
PVA – Polyvinyl Alcohol

Chapter 1

Introduction

The acceleration of ions and subatomic charged particles is of great importance in many fields of science, engineering, and healthcare, involving the interaction of such radiation with matter in ordinary states or with other high-energy beams.

The classical technology of acceleration consists in using of electromagnetic systems (composed of electrodes, coils, magnets) which have relatively large size for a given gain of particle kinetic energy. This is the downside of the long chain of successive electromagnetic devices required by the classical accelerators. Because of these facts, an optical technology for the acceleration of charged particles has started to develop in the recent decades, involving HPL sources (laser-driven acceleration) which their powers have relatively rapidly increased in the last decades due to the introduction of the chirped pulse amplification technique [1] [2]. This uses a focused HPL pulse in interaction to targets in gaseous, solid, or liquid state. After this fast interaction, high flux of accelerated charged particles is generated practically instantaneously from the target. These particles are positive ions and electrons that are delivered from the ionization process of target atoms triggered by the extremely electric field of laser pulse in the focus point. The kinetic energy of these particles can reach values in the relativistic range (hundreds of MeV/u for ions [3]), even ultra-relativistic for the electrons. A major advantage of this novel acceleration technology is the very high ratio of kinetic energy gain to the acceleration path length of particles, which is made possible by the high electric field strength in the focus (even $10^5 \div 10^6$ times higher than the electric field in conventional accelerators) [4] [5]. Another key advantage of such systems is the perspective of scale reduction (table-top laser-driven accelerators), the entire experimental assembly becoming more compact than another based on the classical accelerator [3]. Last but not least, strong secondary electromagnetic radiation is simultaneously generated during the acceleration (e.g.

extreme-UV, X-rays, even gamma rays), useful for other applications requiring radiation in these spectral ranges.

Using thin solid films as targets for HPL pulses, accelerated ions can be obtained at higher energies than using thick solid films [6]. The target films must be made of compounds containing atomic species that will be accelerated as positive ions.

Many types of ionic species can be used in experiments in different fields (e.g. nuclear physics, radiation shielding materials, hadron therapy, radioisotope production, industrial proton imagery, experimental astrophysics) [7] [8]. Of these, the accelerated carbon ions are a special category, particularly because of their usefulness in new high-energy carbon ion radiotherapy against some types of tumours [9]. High-energy positive ions (including carbon ions) have the property that the absorption of kinetic energy by the propagation medium (tissues) is inversely proportional to the instantaneous kinetic energy, so that chemical damage in the propagation medium will be proportional to depth [10]. This helps to minimise damage to healthy tissues (placed before the tumour) and maximise tumour destruction [11]. There are few applications of laser driven ions/protons which are given importance also, such as the fast ignition fusion, the exotic particles generation, and the reconstruction of the accelerating electric fields dynamics by the proton emission measurements [12].

Carbon can exist in a solid state at normal temperatures, which means it can be used in solid films for laser acceleration experiments. Thin films of tens/hundreds nanometers thicknesses can be grown by deposition techniques using a substrate. Because only the carbon layer is required in the laser focus spot, the film in freestanding form is required [13] on areas of at least one square-millimeter in order to protect the substrate against damage caused by high electric currents induced in the film around the focus zone when interacting with the HPL pulse. This means that the size of film freestanding area is much larger than the film thickness (high-aspect ratio) [14]. Thus, the risks of shearing and scratching of the freestanding film caused by external or internal mechanical forces up to the moment of HPL interaction are present during target handling, target storage, and after target mounting. For this reason, it is necessary to use a film with good mechanical properties (e.g. high tensile strength, high hardness). Carbon is suitable for these mechanical requirements due to the possibility to grow into DLC or diamond or graphene forms, using suitable deposition processes. These types of carbon materials are known to have good mechanical behaviour. There is already commercially available substrate-less DLC foils with thicknesses from half of or one micrometer to tens of micrometers or more, usable in the laser-driven ion acceleration experiments. Instead, the thickness ranges from nanometers or tens of nanometers to hundreds of nanometers are uncovered by this kind of providing. Even though its might be covered a little under half a micrometer, anyway the substrate-less foils with submicrometric thicknesses are very difficult to manipulate, with integrity preservation, to fix on the target holders. Therefore, the development of substrate-using methods for DLC film growth is stringent even this way involves the substrate etching to attain its freestanding form. On the other hand, an on-site fabrication chain is thus implemented within the laser-driven facility, mitigating the out-sourcing dependence, and even the long delivery times, which an off-site chain generates. This thesis presents a development which meets such desiderates, wherein

DLC targets were studied in terms of fabrication, characterization, and application in HPL experiments. PECVD deposition processes were used to grow DLC thin films with thicknesses of 10 nm ÷ 600 nm in order to compare their characterization results in terms of the films' agreement with HPL experimental requirements.

The DLC films grown on substrates were integrated on target holders in order to use in HPL experiments performed within commissioning campaign of ELI-NP 1 PW experimental area [15] [16] [17] [18]. The experiment in which a fabricated and characterized DLC target was involved has concerned on the laser-driven acceleration of carbon ions and protons regarding the reached kinetic energies [16] [17]. Another previous experiment concerned on the influence of the DLC film on the HPL pulse contrast in double-layer targets as measured by light reflection [18].

Through the chapters which form the thesis structure, the content first defines the general and theoretical framework involved in the research presented. After, the experimental activity and results are discussed, starting with the optimization of the DLC deposition process and continuing with the implementation of this deposition method on copper substrates, the DLC freestanding achievement on these coated substrates and the involving of such DLC/Cu composites in HPL target applications.

Chapter 2

Theoretical framework and methodology

HPL-driven acceleration is a complex process based on laser-plasma interaction phenomena. There are several possible mechanisms of this process in the solid targets. The prevalence of some mechanism or other, as well as the combination of these, depend on certain experimental conditions which also can influence the mechanism efficiency, the flux characteristics and the energy spectra of accelerated particles, such as: the thickness of target film, the mass and charge distributions of electrons and nuclei inside the target, the presence or not of nano/micro-structuration, the incidence angle of HPL, the intensity and polarization of incident HPL pulse, the contrast ratio between the main pulse and pre-pulse/pedestal, and the HPL beam profile. There are two distinct and main acceleration mechanisms (regimes), TNSA and RPA, the first one being early and most investigated within laser facilities [19] and the second one more later because of more restrictive requirements for laser pulses, i.e. intensities and contrasts higher with several orders of magnitude than for TNSA, such capabilities emerging more recently, especially with the development of petawatt-class lasers. There are intermediary regimes which could extend the cut-off ion energies of TNSA, e.g. RIT, BOA, RPA-TNSA [7] [20], using thin and very thin targets until nanometric thicknesses [16].

Apart from crystalline structures, carbon can form some amorphous materials that contain atoms in one or more hybridization states (mixture of hybridization states). An example of such material is represented by DLC (amorphous mixture, composed predominantly of sp^3 carbon and less of sp^2 carbon, the ideal DLC entirely containing sp^3 atoms) [21] [22].

The diamond, DLC and graphene can be grown in thin films and exhibit good mechanical behavior [23] [24]. The DLC exhibits an amorphous structure [21] that lacks

the long-range crystalline order and a lower brittleness in comparison to the diamond and graphite, merging the flexibility with the high hardness provided by the sp^3 C-C bonds [25] [26]. Other materials which manifest high mechanical rigidity show the brittleness, not so appropriate to use where good mechanical properties are required. This amorphous carbon material can be grown by PECVD techniques [21] [27] requiring temperatures below 300ºC, lower than those required in the CVD depositions of the diamond and graphene, allotropes with long-range crystallinity. The PECVD deposition of DLC films has the advantage of being suitable with almost any substrate which is vacuum compatible.

The DLC can be grown via hydrogen high-consuming processes (e.g. CVD), which may result in an unneglected content of this element in films (hydrogenated DLC). Regarding the use for laser-driven acceleration, such targets could provide proton-enriched beams besides carbon ions. This supplementary proton flux is added to those emitted from the surface impurities layer which is inherently while the grown film surfaces come in the contact with the atmospheric traces of H_2O and C_xH_y pollutants since the deposition chamber venting until the vacuuming of HPL interaction chamber which is one step in the whole chain of target use.

In this thesis, the main goals have been the growth and analysis of carbon thin films for laser-driven ion acceleration experiments. For HPL applications, it is necessary to use films that meet specifical geometric, mechanic, chemic and morphologic conditions [16]. Here is proposed a DLC targets configuration where the film is partially supported by the substrate, having freestanding zones surrounded by the non-freestanding region [16].

A size of 1 mm for the freestanding zone is large enough to avoid the substrate damaging which occurs because of the HPL pulse - freestanding film interaction [16] [17], and small enough to avoid too high mechanical risks of a very high aspect ratio even for robust films [16] [22] [23] [28] [29].

Regarding the morphology, a roughness constraint accordingly with the Rayleigh criterion [30] is required to assure the prevalence of specular pulse propagation through the solid DLC film when the incidence starts. In order to consider the reflection surface enough smooth to prevail the coherent component of the reflected electromagnetic wave [31], the Rayleigh roughness parameter (Ra_r) of the surface is restricted to maximum 0.8 by Rayleigh criterion for normal incidence [30]. This criterion is applicable when the light passes the surface, using for transmission a similar parameter (Ra_t) which also involves an upper limit [30]. This case is available here while the pedestal absorption starts along the transmission paths in film, sustaining the preplasma formation. The absorption volume is more compact and more delimited once the diffuse transmission is minimized. In Equation (2.1) [16], the Ra_t depends on the R_q roughness [30] through the reduction factor p for the considered λ once $R_q=\lambda/p$, on the refractive indexes of the PECVD-grown DLC which is called as $n(\lambda)$ and considered in interval of 1.57÷2.32 for visible middle wavelength [32], and of the vacuum front medium which is equal to 1 [16]:

$$\mathrm{Ra_t} = \frac{\pi|1 - \mathrm{n}(\lambda)|}{\mathrm{p}} \tag{2.1}$$

A maximal value of $\lambda/10$ for roughness R_q [22] [23] [28] [29] was choose to overcover enough multiple cases for the Rayleigh criterion at normal incidence [16]: the interval of $\lambda/5.3 \div \lambda/2.3$ for transmission through DLC according with Equation (2.1); $\lambda/8$ for reflection [31]. The last case is considered for sacrificial plasma mirrors, other applications of thin films in HPL experiments (apart from target applications) which could furturely benefit from the fabrication and characterization methods presented in this thesis [16]. This application is useful for the contrast enhancement of laser pulse and the protection against back-reflection and debris [33] [34]. In view of the above, the final roughness limit that the fabricated films must meet for any HPL application was set more restrictively than for the target applications which only requires the Rayleigh criterion for transmission. During the research conducted for this thesis, the concern was the HPL target applications. In the case of HPL pulses generated by the Ti:sapphire laser system from ELI-NP, λ is close to 810 nm [15] [35] [36], thus the upper limit for the film roughness in this case is ≈81 nm, the value considered in this research work.

On the basis of above and the required thicknesses to achieve the maximum average kinetic energy of carbon ions (≈80 nm for λ=820 nm and I=5×10^{22} W/cm^2) [20], the high sp^3-content carbonic films are required. The DLC allows to meet the thickness requirements, the reason for choosing this material here.

To achieve high mechanical strength values of sp^3-sp^2 mixtures (e.g. DLC), we assume that it is necessary to grow films with high sp^3-content. This is an aimed chemical condition derived from the mechanical requirement mentioned above.

Geometric configuration of DLC freestanding zones requires an alternant feature [37], where non-freestanding film completes the substrate surface between freestanding zones.

For λ=810 nm, the best focus spot (minimum size) has a diameter of d=1.2·λ≈1 μm, considering the diffraction limit of laser pulse.

DLC films can be deposited on a substrate using high-vacuum plasma processes. In these processes, a precursor gas mixture is introduced into the vacuum chamber at controllable partial flows. One of the gases in the mixture must contain the carbon element that will be the source of the grown carbon layer (this gas is usually a hydrocarbon) [23]. The other gases of the mixture can be an inert gas (e.g. argon) and/or diatomic hydrogen.

During the PECVD growth of DLC films, sp^2 and sp^3 carbon structures are formed simultaneously in the deposited material. The hydrogen ions from the formed plasma play an important role in etching sp^2 carbon structures at higher rates than for sp^3 carbon structures [38] [39]. This fact favors the formation of sp^3 structures to the detriment of sp^2 structures [24], which is exactly the proposed goal. The hydrogen element involved in these two etching processes comes from hydrocarbon gas and from H_2 when it is used [38]. On the other hand, small amounts of hydrogen from the plasma could be embedded in the grown films [40], this contamination being useful for experiments of HPL acceleration of hydrogen ions with mass number A=1 (protons) besides of carbon ions [41].

On the other hand, the maximum deposition area using this technique can be large, depending on the electrode sizes, which is useful for growing films for HPL target applications (centimeter order size of the deposited film is required to ensure a sufficient number of freestanding zones on the same substrate after further back-etching).

Gaseous precursor mixtures containing carbon combined with hydrogen and/or oxygen elements are referred by the C-H-O diagram (see Figure 2.1), which is available for general CVD processes, involving plasma or not (PECVD also included). Visually, this diagram consists of an equilateral triangle with each corner named like each chemical symbol of these three elements. The diagram has three coordinates corresponding to one point on each side of the triangle [42] [43]. These coordinates are called X_{HC}, X_{OH} and X_{CO}, and are defined by Equation (2.2) [42] using the compressed notation $X_{HC;OH;CO}$. This diagram indicates which C:H:O stoichiometries of the gaseous precursor mixture are favorable for the growth of sp^3 carbon structures in carbon films during CVD deposition processes.

$$X_{HC;OH;CO} = \frac{N_{H;O;C}}{N_{H;O;C} + N_{C;H;O}} \tag{2.2}$$

The quantity N, indexed with C or H or O, represents the total number of atoms of carbon or hydrogen or oxygen in the precursor mixture inside of deposition chamber. With respect to the triangular representation (see above diagram), these three quantities uniquely correspond to three points on the sides of the triangle. In the corner 'C' (carbon) X_{HC}=0 and X_{CO}=1, while in the corner 'H' (hydrogen) X_{HC}=1 and X_{OH}=0; also, in the corner 'O' (oxygen) X_{OH}=1 and X_{CO}=0. Along the triangle sides, the coordinates linearly vary such that in the corners they take the previously mentioned values. The point (state) in this diagram is obtained by the intersection of three lines, each defined by a coordinate point and its opposite corner [42].

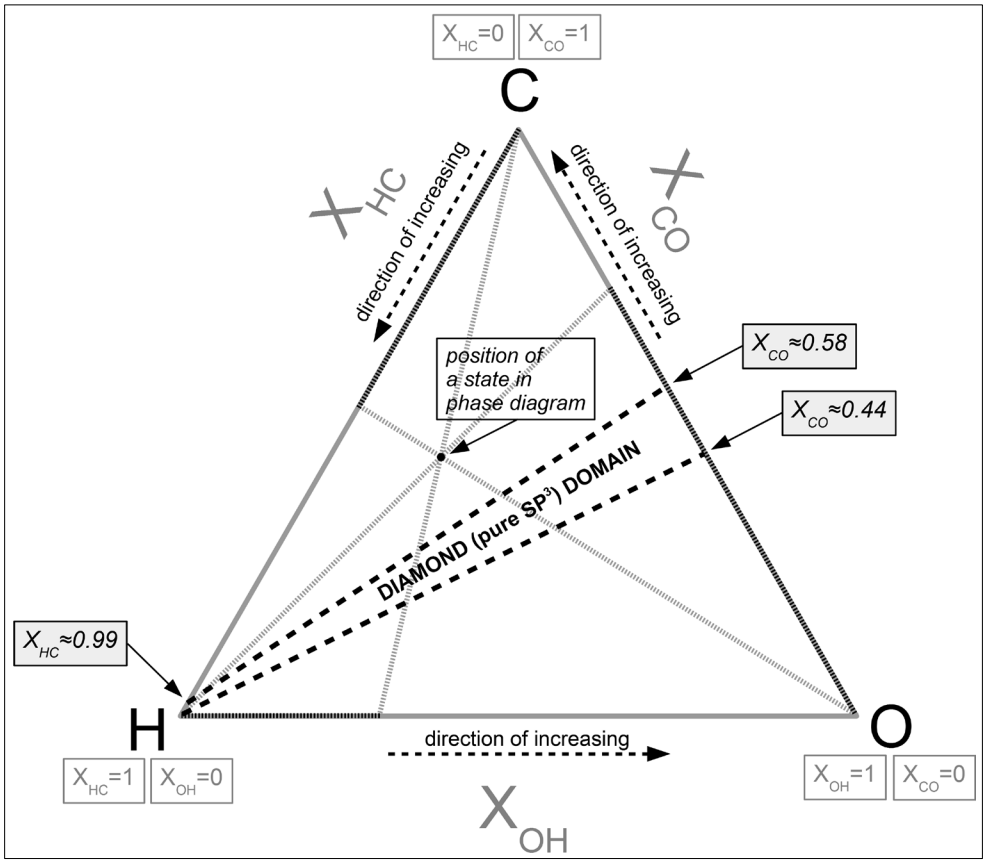

Figure 2.1: *Geometrical representation of C-H-O diagram (equilateral triangle); redrawn after a figure from the bibliographic reference [42]*

In the geometric representation, X_{HC} , X_{OH} , and X_{CO} correspond to the distance between the coordinate points and the 'C', 'H', and 'O' corners, respectively. In the same representation, $1\text{-}X_{HC}$, $1\text{-}X_{OH}$, and $1\text{-}X_{CO}$ correspond to the distance between the coordinate points and the 'H', 'O', and 'C' corners, respectively.

At a given temperature, if the partial pressures of gas components are equal then their molecular concentrations (number of molecules per volume) also are, under the ideal gas law (further, these equal concentrations will be addressed as n^*). Such condition for partial pressures was applied in the DLC growth process developed within our research. The number of atoms for each element from the precursor mixture depends on the atomic stoichiometry and gas flow for each component molecular species (the i^{th} molecular species is labeled with M_i for $i = \overline{1,q}$, where q is the total number of species). Also, it depends on the gas component concentration n^* and on the deposition time Δt which also is same for each M_i. These dependencies are expressed in the following equation:

$$N_{C;H;O} = n^* \cdot \Delta t \cdot \sum_{i=1}^{q} N_{C;H;O}(M_i) \cdot \Phi_{M_i} \quad , \qquad (2.3)$$

where Φ_{M_i} is the gas flow (volume per time), while $N_{C,H,O}(M_i)$ is the number of C or H or O atoms in one M_i molecule.

Equation (2.3) is useful to obtain the aimed stoichiometric ratio of the precursor mixture (reciprocal ratios between N_C , N_H , and N_O) by using appropriate ratios between the set flows of gases forming the precursor mixture.

At the same time, it is necessary to maintain a total pressure in the chamber during the deposition process that is favorable for film growth. The required C:H:O stoichiometry directly determines only the ratio between the flows of component C/H/O gases, not their values. Thus, the total pressure and the reciprocal ratios between the flows of C/H/O gases are critical to the growth process.

The stoichiometric ratio is related to triangle diagram coordinates, thus the required gas flows are determined by knowing the X_{HC} , X_{OH} and X_{CO} coordinates that need to achieve on diagram and the chemical element stoichiometry of component gases. In the Figure 2.1, the superior and inferior limits inside diagram, corresponding to the pure sp^3 carbon structures (like diamond) in the grown carbonic films, are shown in black discontinue lines. Each of these lines meets each of [CH] and [CO] triangle sides in one point as follows: the superior line between X_{HC}=0.99 and X_{CO}=0.58, and the inferior line between X_{HC}=1 and X_{CO}=0.44. Therefore, the growth of high sp^3 carbon films is involving the coordinates from mentioned region [42].

Patterning of substrates is required after the film deposition stage to obtain a freestanding film structure, using a procedure based on UV-lithography and back-etching in $FeCl_3$, suitable for copper substrates [23].

Once the targets are fabricated, it is necessary to verify their compliance with the required properties [16] using characterization techniques specific to materials science.

The step-height method is a way to determine the thickness of a film deposited on a substrate. This method is based on the acquiring of a line-profile $z(x)$ that must include

both the uncoated and coated areas of the substrate (this profile is also called 2D profilogram). From the obtained linear profile, an interval is selected in the uncoated zone and another in the coated zone to calculate their z averages: $\bar{z}_{\mathrm{uncoated}}$ and $\bar{z}_{\mathrm{coated}}$. The thickness associated with a line-profile is considered to be the difference (step-height) between these averages [22] [28] [29]: $\mathrm{h} = \bar{\mathrm{z}}_{\mathrm{coated}} - \bar{\mathrm{z}}_{\mathrm{uncoated}}$. The contact profilometer is an instrument used for such measurement because of the ability to scan a line-profile even along few millimeters, taking into account that it is necessary to include in the scan line at least the entire cross-zone between the uncoated and coated substrate.

Film thicknesses determine the deposition rate of DLC growth in specified conditions, extracting this rate by the linearly fitting of the experimental graph of thickness vs. deposition time plotted in the base of grown films.

The asperity of a material surface is quantified by the roughness parameter which characterizes the topography of the scanned zone. After this scanning which is performed with profilometer tools (e.g. optical profilometer, AFM microscope), a 3D profilogram $z(x,y)$ is generated where z is the height level of the point on the scanned surface [23]. In Equations (2.4), the S_q quantity (the RMS 3D roughness) is defined accordingly to the ISO 25178 standard. The $M{\cdot}N$ product is the count of (x_i , y_i) pairs corresponding to the z measurement points from the rectangular scan zone, after the Oz translation of profilogram with $\Delta z=|z_{average}|$ toward the origin of axis. Another function which characterizes the topography is the line-profile $z(u)$ with u the coordinate along it. The R_q quantity measures the 2D roughness of line-profile, being defined like S_q as in Equations (2.4), where P is the count of u_k coordinates of points from profile after the translation abovementioned. The line-profiles can be directly acquired by a profilometer equipment or extracted using software from an acquired 3D profilogram. The extraction of profiles in the latter case can be useful to measure the roughness on a region of interest more restricted in size than the acquired large area profilogram, the more so as if the surface presents a waviness feature on the scanned area.

$$\mathrm{S_q} = \sqrt{\frac{1}{\mathrm{M}\cdot\mathrm{N}}\sum_{\mathrm{i,j=1}}^{\mathrm{M,N}} \mathrm{z}^2(\mathrm{x_i},\mathrm{y_j})} \quad , \quad \mathrm{R_q} = \sqrt{\frac{1}{\mathrm{P}}\sum_{\mathrm{k=1}}^{\mathrm{P}} \mathrm{z}^2(\mathrm{u_k})} \qquad (2.4)$$

The ratio of sp^3 and sp^2 hybridization states of carbon in the characterized films will give an indication of the behavior under mechanical stress that may occur during manipulation of aggregates containing the film in freestanding form. Regarding the acceleration process, the concentrations of the ion species of the emitted flux will depend on the elemental composition of target film, besides its thickness, density, the HPL pulse parameters and other laser-target interaction conditions. Therefore, the DLC films require chemical characterization which can be performed by XPS to determine the carbon hybridization ratio and by EDX for the composition of chemical elements.

The XPS is a quantitative analyze technique for the sp^3- and sp^2-carbon concentrations of thin carbon films [23]. It is assumed that DLC films have higher mechanical strength than poly-amorphous graphitic films, therefore it will follow to grow DLC films with

high-concentration of sp^3 carbon. Thus, XPS is a way to check the quality of growth process in terms of diamond/lonsdaleite abundance in the grown films.

The peak area is directly proportional to the content of the corresponding allotropic form, allowing the determination of the allotropic percentage concentration of the analyzed atomic species. Peak positions in XPS spectra are around 284.4 eV for sp^2-carbon [44] and higher with 0.6÷0.9 eV for sp^3 carbon [44] [45].

The EDX is a semi-quantitative analysis technique for the concentrations of atomic species inside the grown thin films, which is a supplemental functionality of the scanning electron microscopy.

Chapter 3

Fabrication and characterization of DLC films on Si substrates

Next, the carbon film growth experiments are presented, performed toward the achievement of preceding mentioned goals of this thesis, regarding the thickness, roughness and sp^3- to sp^2-C ratio.

In order to focus this development only on the parameters of growth process itself, clean substrates with very smooth surfaces (Si wafers) were used. This choice has allowed to exclude a worse substrate roughness as the cause of a worse film roughness if such an event would have occurred.

The PECVD technique with radio-frequency power supply (100 W at 13.45 MHz) and high-vacuum pumping was used to grow two sets of thin carbon films (DLC) under different conditions at INFLPR. The metal holder was floating and spun at 100 rot/min throughout the process to increase the spatial uniformity of the deposited film. Prior to being held in the chamber, the substrates were partially covered with a mask to leave an uncoated zone on the substrates after the process, which is useful for determining the film thickness by the step-height method. Previously of the deposition process, a plasma treatment was performed on the substrates for 10 min under the same conditions as the subsequent deposition (power, radiofrequency, and holder spin speed), but in Ar/H_2 low pressure atmosphere (20 sccm flow for each gaseous species). In the literature this is reported as a method for the surface impurities removal [27], leading to a better adhesion of the grown film.

The PECVD process conditions used in the experiments are given below for each set of samples (set I, set II) [22] [28] [29].

Set I has consisted of two samples whose substrates have contained silicon with [001] crystallographic orientation. The precursor gas mixture has contained CH_4 and Ar

(Φ_{CH_4}=25 sccm, Φ_{Ar}=50 sccm) with a C:H carbon/hydrogen stoichiometry of 1:4 calculated using the preceding Equations (2.2) and (2.3).

For set I, the total pressure inside the chamber was $p \approx 10^{-3}$ mbar during the deposition process. The deposition time was different for each of these samples. These chosen Δt values were 200 min and 300 min.

Set II has consisted of four samples whose substrates has contained silicon with [001] crystallographic orientation. The precursor gas mixture has contained CH_4 and H_2 (Φ_{CH_4}=25 sccm, Φ_{H_2}=62.5 sccm) with C:H carbon/hydrogen stoichiometry of 1:9 calculated in the same manner as for set I.

For set II, the ratio between the flows of C/H containing gases was Φ_{CH_4} / Φ_{H_2}=0.4 and the total pressure inside the chamber was $p \approx 1.5 \cdot 10^{-3}$ mbar during the deposition process. The deposition time was different for each of these samples. The chosen Δt values were 23 min, 34 min, 45 min and 60 min.

KLA Tencor-P7 contact profilometer was used at INFLPR to determine the thickness by the step-height method. The step-height value for each DLC sample is mentioned below [22] [28] [29]. Also shown are the calibration curve and the deposition rate of the growth processes for each set that had different process parameters [22] [28] [29].

For the set I samples, the line-profiles were acquired, being at the base of determined thicknesses which was found 381.7 nm and 535.5 nm for Δt=200 min, and respectively, Δt=300 min, with the error of 18.8 nm, and respectively, 107.2 nm.

By linearly fitting the experimental points, the process calibration curve (Figure 3.1) was found, resulting in a deposition rate (the linear slope) of 1.8 nm/min for the growth process of set I samples.

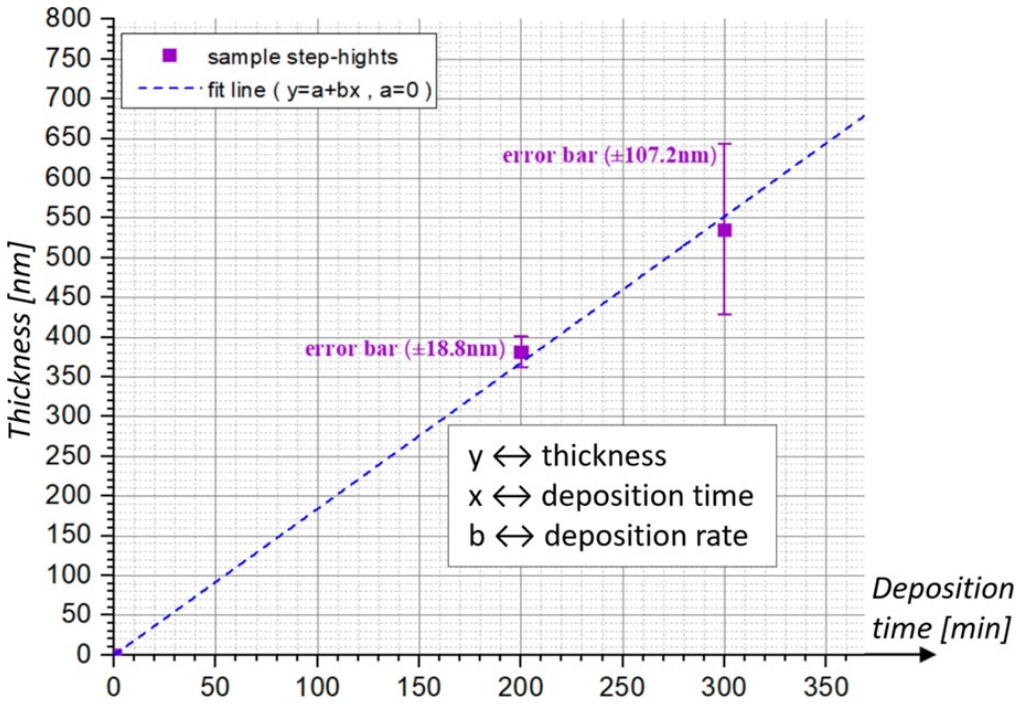

Figure 3.1: *Process calibration curve f(x)=b·x for set I; thicknesses are step-height values*

For the set II samples, the line-profiles were acquired, being at the base of determined thicknesses which was found 21.8 nm, 26.4 nm, 50.5 nm and 57.4 nm for Δt=23 min, Δt=34 min, Δt=45 min, and respectively, Δt=60 min with the error of 6.8 nm, 12.2 nm, 11 nm, and respectively, 6.8 nm.

By linearly fitting the experimental points, the process calibration curve (Figure 3.2) was found to have the linear slope of 1 nm/min (the deposition rate) for the growth process of set II samples.

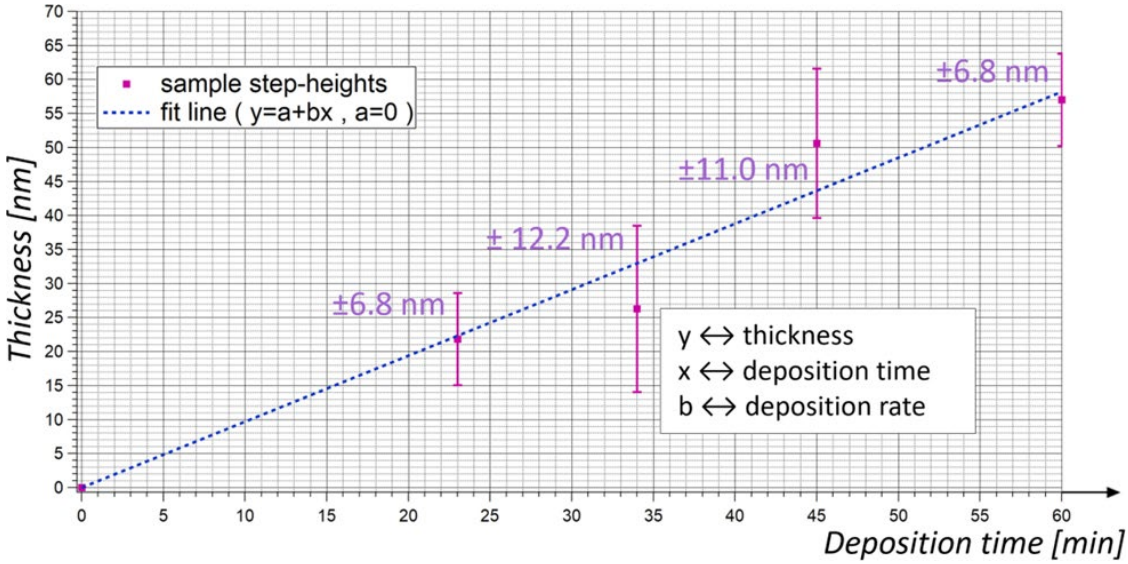

Figure 3.2: *Process calibration curve f(x)=b·x for set II*

The AFM 3D profilograms were acquired at ELI-NP with the microscope NT-MDT Ntegra, scanning over 5×5 μm^2=25 μm^2 on grown film surface of each sample from each set, finding for set I the root mean square roughness (S_q) of 1.2 nm and 2.3 nm for Δt=200 min, and respectively, Δt=300 min, and for set II the roughness of 3 nm, 0.2 nm, 0.5 nm and 0.2 nm for Δt=23 min, Δt=34 min, Δt=45 min, and respectively, Δt=60 min [22] [29].

The optical 3D profilograms were acquired at ELI-NP with the profilometer Sensofar S Neox, scanning over ≈351×264 μm^2=92664 μm^2 on grown film surface of each sample from each set, finding for set I the root mean square roughness (S_q) of 18.6 nm and 14.8 nm for Δt=200 min, and respectively, Δt=300 min, and for set II the roughness of 2.9 nm, 2.7 nm, 1.6 nm and 1.9 nm for Δt=23 min, Δt=34 min, Δt=45 min, and respectively, Δt=60 min [22] [29].

The chemical analysis of carbon films, in terms of sp^3- and sp^2-carbon composition, was performed by XPS using the ThermoFisher Scientific ESCALAB^{TM} XI^+ instrument at INFLPR. The representative spectra for each set of samples was Voigt fitted in concordance to the carbon allotrope sp^3- and sp^2-peaks, the ratio of the area of each peak to the area of all peaks being the percentage concentration of each allotropic form in the DLC film, which for sp^3 and sp^2 was found 21.1% and 78.9% (set I), and 45.5% and 54.5% (set II) [22] [28] [29].

The sp^3 vs. sp^2 hybridized C content has been improved, as implying a better mechanical strength of DLC films in the freestanding form. On the other hand, according to the data presented above of this chapter, the ratio of DLC roughness to HPL wavelength ($\lambda \approx 810$ nm for ELI-NP) were very satisfactory ($\sim 10^{-4} \div 10^{-3}$) and the roughness compliance with the upper limit of $\lambda/10 \approx 81$ nm was also very good. This topographical characteristic stands out on scan areas at least of the same magnitude order (AFM) or much larger (optical profilometry) than the diffraction limit of the HPL focus spot size (≈1 μm for this λ). The above results reveal that the PECVD process was well optimized to obtain the DLC thin films meeting the requirements for the experiments of laser-driven acceleration from ELI-NP.

Therefore, the DLC deposition method corresponding to the set II was selected for the growth on copper substrates toward to achieve the HPL targets. The reason for use the copper substrates consists of the wet chemical route availability for substrate back-etching, thus not being necessary a complex equipment like the reactive ion etching if silicon substrates had been used, especially since the latter technique needs high-pressure recipients filled with the environmental hazardous fluorinated gases [46] leading to an exhaust filtration requirement. Another reason is that the control of the corrosion stop moment is not required due to the lack of reactivity between the etch reagent (e.g. iron chloride) and the deposited carbonic film, instead for reactive ion etching it is because of plasma reactivity with both silicon substrate and carbonic film [46]. Thus, the stopping of the reactive ion back-etching process is mandatory to exactly be after the going through the substrate, while the wet etching process not requiring this.

Chapter 4

Freestanding DLC films on unpolished Cu substrates etched by UV-lithography. Target assembling

This chapter is concerned on the realization of freestanding carbon (DLC) films on substrates mountable on metallic frames for using in experiments with high-power laser pulses to elucidate some aspects of the interaction between low-contrast laser pulses and solid targets without using any plasma mirror [18]. The DLC films self-supporting (freestanding) on perforated Cu substrates were mounted on metallic frames with Al foils previously fixed, to form DLC-Al double target ensembles. The Cu substrates are much easier to process than Si substrates, benefiting by simple chemical routes for etching and, supplementary, manifesting ductility which favours the mechanical integrity of substrates during processing.

The double target ensemble (Figure 4.1) [18] has consisted of a foil bonded to a perforated Al frame, spacers bonded to the foil, and a patterned DLC/Cu sample bonded to the spacers, contacting the DLC side so that the Cu substrate hole is aligned with the foil and frame hole. In this case, the Al foil is the target itself, the matte surface of foil is the front surface, and the shiny surface is the rear surface (the positioning of foil surfaces does not matter if these do not visually exhibit matte or shiny characteristics). In such an experiment, C and H ions are accelerated from the rear foil contaminants [41]. To increase the efficiency of acceleration process, the HPL pulse hitting the foil must have a higher contrast. This can happen if a thin solid film turns into a plasma and absorbs much of the pre-pulse energy, then the plasma dissipates before the main pulse arrives, and the enhanced-contrast pulse hits the foil after traveling tens of microns [18]. Such a

phenomenon could occur in a spaced bilayer structure consisting of a thin solid film in front, an empty space with thickness of tens of micrometers, and a foil in the rear, focusing the HPL pulse on the front side of foil [18]. This structure is fulfilled in the target ensemble above mentioned.

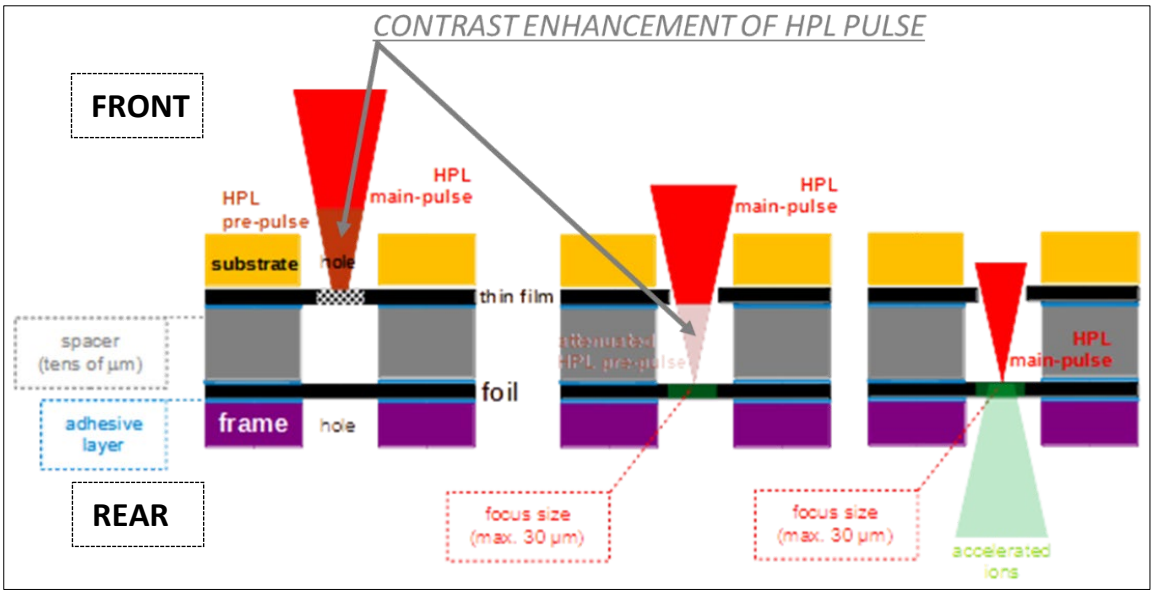

Figure 4.1: *Sketch of double target ensemble in acceleration experiment (transversal view)*

The content of this chapter is related to the achievement of freestanding DLC films deposited on Cu substrates, as follows:

- preparing of Cu substrates (debiting, deposition-mask mounting, clean);
- DLC films growth on Cu substrates (the obtaining of DLC/Cu samples);
- Cu substrates patterning in $FeCl_3$ aqueous solution bath;
- characterization (thickness determination, optical microscopy, optical profilometry).

The patterning of Cu substrates was performed after different tests with or without DLC film (preliminary experiments), then the best variant was selected, which is described below (UV photolithography involved):

a) the spraying and drying of positive photoresist layer on each side of DLC/Cu sample;
b) the patterning of photoresist layer by the UV photolithography using UV-mask and developing process of photoresist layer;
c) wet-back-etching of Cu substrate accordingly with the pattern of UV-mask; wet clean of remaining photoresist.

Next, this chapter is concerned with the achievement of freestanding DLC films on substrates that can be mounted on metallic frames, which can be used in high-power laser experiments. The DLC films were self-supporting (freestanding) on back-etched Cu substrates, which were mounted by gluing with PMMA on Al frames, forming the double target ensembles (Figure 4.1). The preparation of Cu substrates, the growth of DLC films

on Cu substrates (the obtaining of DLC/Cu samples), the back-etching of Cu substrates with DLC films using UV photolithography, and the mounting of such processed DLC/Cu samples on Al frames are presented and discussed.

Before DLC film deposition on Cu substrates, these were prepared so that to ensure sizes of DLC/Cu samples which allows easy manipulation during entire fabrication chain, to ensure good quality of growth surface and to ensure lateral undeposited region to avoid peeling off which could start from substrate boundary during wet processes involved in fabrication. Substrates were cut from A4 format Cu foil (100 µm thickness) in ~ 30 mm × 20 mm pieces, then were mounted, not being polished, in the deposition frame and ultrasonic cleaned in IPA with the frame together before DLC growth, the frame being removed after growth, so the DLC/Cu sample has resulted. The DLC films were grown at INFLPR on such mounted substrates, by PECVD using C/H gas mixture precursor with high H content at the total pressure of ~10^{-3} mbar, in radiofrequency electric field of 13.56 MHz and 100 W power [18]. Batches of six DLC/Cu samples were obtained, each batch in one growth process, having samples with same thickness of DLC film. The sample label is formed by its batch label followed by a number from 1 to 6.

The thickness was determined by mechanical (contact) profilometry (step-height method) at INFLPR. For this determination the substrate was partially covered during the film growth process, thus the film edge is just the step between the substrate and film.

The DLC film thicknesses were found as follows: 129 nm, 67 nm, 163 nm, 64 nm, 208 nm, 42 nm and 78 nm for batch A, B, C, D, E, F, and respectively, G.

The patterned back-etching [17] [18] has followed the frame unmounting.

The designed pattern of UV mask has consisted by 10 cylindrical holes [17]. Mask holes were labeled from H1 to H10, keeping the same labeling on Cu-side of DLC/Cu sample for substrate holes. Labeling of freestanding zones on DLC-side of DLC/Cu sample is that of corresponding holes on the Cu-side.

Characterization by optical microscopy on the Cu side was made on the samples after the acetone rinse step (the photoresist removal) [17]. After the etching process of substrate, the DLC film has become visible on the fully corroded (empty) holes, being in the freestanding form. The average size of each full-corroded hole (average of the size values measured on that hole) was also measured. Regarding the morphology, on the DLC freestanding surface toward the substrate, striations like those on the substrate were observed. This is explained by the transferring of the morphology of Cu substrate onto the DLC film at the interface to Cu substrate.

The size of the freestanding zone of DLC film is identical to those of the corresponding hole on the back-etched Cu substrate.

Statistics of average sizes were obtained by Excel (minimum of 472 µm, maximum of 1989 µm, mean of 1035 µm, STD of 294 µm, and STD to mean ratio of 28%) [18].

The mean size of all achieved freestanding zones was close to the value of the diameter of UV mask holes (1 mm).

The optical microscopy at 50X magnification on the Cu side of freestanding zones reveals that the substrate morphology (the striations) was transferred to the DLC film. The impurities/traces are present, having as possible sources the photoresist film, the chunks of Cu material incompletely corroded and the $FeCl_3$ solution bath [18]. Generally,

the flat zones lie on the areas of $5\times10^2\div5\times10^4$ μm^2, this means the well-focused surface zones in the images.

Rates of Cu holes completely etched, rates of DLC freestanding zones survived, and combined rates (the combination of these two rates by multiplication), until the optical microscopy investigation which was performed in maximum one day since the corrosion of substrate, were determined. The combined rate for groups of samples (batches) and for all samples (global) were found 53% for B, 88% for E, 68% for F, and 61% globally.

The optical profilometry tool was used to acquire and to untilt the 3D profilograms, and to determine the S_q roughness of freestanding-film on bottom surface (Cu-side), after the photoresist removal, in confocal mode on 175.44×132.10 μm^2 scan area.

The statistics of 3D roughness (S_q) from profilograms acquired on bottom surface of freestanding DLC film was performed. The average, the STD, and the ratio of STD to average were calculated on DLC freestanding zones. For groups of samples (batches) and for all samples (global) were found $S_{q(average)}$=1.5 μm, *STD*=0.7 μm and STD/$S_{q(average)}$=49.2% for B, $S_{q(average)}$=1.6 μm, *STD*=0.5 μm and STD/$S_{q(average)}$=32.3% for E, $S_{q(average)}$=1.2 μm, *STD*=0.8 μm and STD/$S_{q(average)}$=64.2% for F, and $S_{q(average)}$=1.4 μm, *STD*=0.7 μm and STD/$S_{q(average)}$=48.9% for global.

Gwyddion data processing of 3D profilograms acquired on bottom surface of freestanding DLC film was used to check if the surface has the roughness in limit of $\lambda/10\approx81$ nm. One freestanding zone for each batch was selected for this processing. For each selected zone, 3 line-profiles of length of ~100 μm were extracted from its raw (tilted) 3D profilogram [18]. These raw line-profiles were software processed to untilt by subtraction with fit line, following 2D roughness (R_q) calculus [18].

The R_q average for each batch [18] and globally were found 790 nm for B, 706 nm for C, 419 nm for E, 763 nm for F, and 669 nm globally.

The R_q average global is higher than $\lambda/10\approx81$ nm limit (roughness upper limit on zones with sizes which cover diameters domain of all used HPL focus spots; theoretical minimum diameter of focus spot is $1.2\cdot\lambda\approx1$ μm).

The substrates scratches (striations) explain these high R_q-roughness values. Because the substrate morphology is transferred to bottom surface of freestanding DLC, the substrate polishing will be needed to remove the DLC striations and to decrease R_q roughness.

Toward double target ensemble fabrication (Figure 4.1), few steps were used consisting of the fixing the Al foil, the fixing of spacer stack, the cutting and fixing the DLC/Cu samples, obtaining the structure sketched in the Figure 4.2 [18].

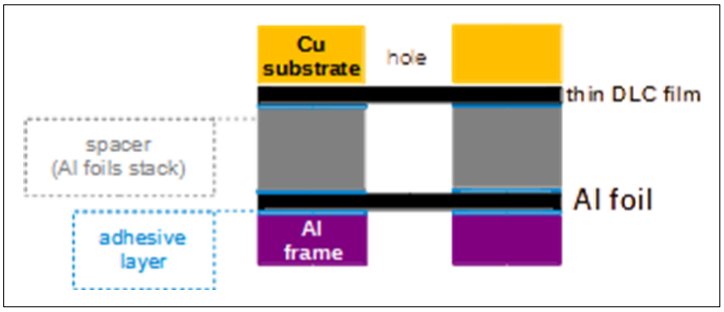

Figure 4.2: *Sketch for double target ensemble*

Each cut fragment has just one usable DLC freestanding zone in HPL target ensemble. Just four of the DLC freestanding zones of a corroded DLC/Cu sample are usable, no matter how many survivor freestanding zones does the sample have over the four. Double target ensembles were fabricated to use in HPL experiments. These ensembles were constructed using Al foil of 15 μm thickness as target itself, spacer of 15 μm, 30 μm and 45 μm thickness, DLC film of 42 nm and 67 nm [18].

Chapter 5

Freestanding DLC films on polished Cu substrates etched by UV-lithography. Target assembling

This chapter depicts the experiments related to the freestanding DLC films on polished Cu substrates etched by UV-lithography and used in target manufacturing. The research activity was concerned onto achievement of freestanding DLC films on substrates mountable on metallic frames, being usable in experiments of laser-driven acceleration of C ions and/or protons.

The DLC films were self-sustained (freestanding) on holed Cu substrates which were mounted with PMMA adhesive layer on metallic frames, obtaining the DLC simple target ensembles.

The simple target ensemble (Figure 5.1) [17] has consisted of a patterned DLC/Cu sample (DLC film previously deposited on a Cu substrate and back-etched with holes after deposition) mounted on a perforated Al frame by bonding the DLC side to the frame so that the Cu substrate hole is aligned with the frame hole.

In this case, the DLC film itself is the target, the film surface that was in contact with the etched substrate is the front surface with respect to the HPL pulse incidence, and the opposite is the rear surface. In such an experiment, C and H ions are accelerated. The C ions come mainly from the DLC film and, also, from the rear surface impurities. The H ions also come from the rear impurities and may also come from the residual composition of DLC film. These consist of H_2O and C_xH_y compounds (hydrocarbons) adsorbed from the air or left on the surface of targets after the manufacturing steps [41], which dissociate to chemical elements during the occurrence of preplasma from the solid film target as a

result of the laser pre-pulse incidence. Thus, the ion species of preplasma will be found in the high-energy beam emitted at the laser main pulse incidence which induces the acceleration process.

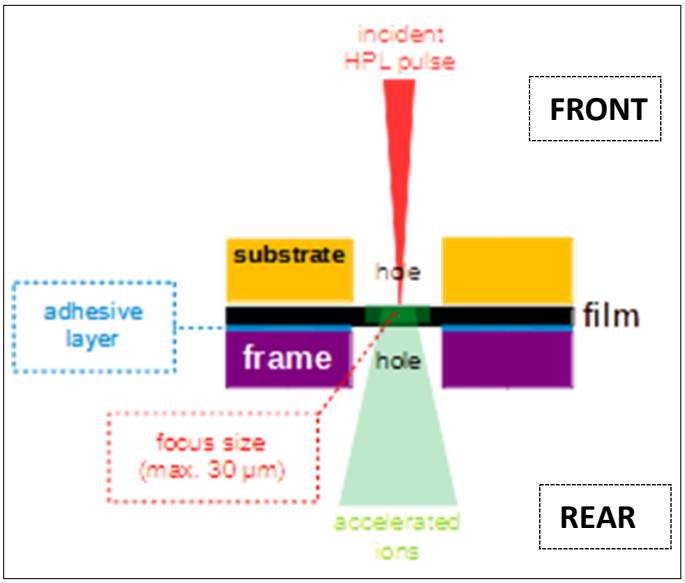

Figure 5.1: *Sketch of simple target ensemble in acceleration experiment (transversal view)*

In this chapter is presented and discussed the HPL targets fabrication and characterization involving other series of DLC/Cu samples, but having polished Cu substrates, by following the themes below:

- preparing of Cu substrates (debiting, flattening, polishing, deposition-mask mounting, clean);
- DLC films growth on Cu substrates (the obtaining of DLC/Cu samples);
- Cu substrates patterning in $FeCl_3$ aqueous solution bath;
- characterization (thickness determination, optical microscopy, optical profilometry, EDX);
- integrating of DLC/Cu samples in the metallic frame;
- HPL acceleration results for carbon ions and protons using this target ensemble.

Before DLC film deposition, Cu substrates were prepared in the same manner as described previously in the Chapter 4, but after the cut from A4 format Cu foil the mechanical (machine) polishing was applied on the surface designated for DLC deposition, and additional preparation steps were done before the mounting of DLC-deposition frames. The polishing has consisted of the preparing and attaching to the polishing holder the Cu substrates, the adhesive curing, the machine polishing itself, the clean and dry of polished substrates on holder, the coating of well-polished surfaces (substrates) on holder with protective layer, and detachment and drying of polished substrates from the holder [16] [17].

After the polishing operation, the protective layer removal and clean were done on the substrates before mounting frames [16] [17].

After the mounting of frames, the DLC film deposition on polished Cu surface [16] and the step-height method were performed at INFLPR as described in the Chapter 4, except that other thicknesses were obtained and determined. Batches of six DLC/Cu

samples were obtained, each batch in one growth process, having samples with the same thickness of DLC film. For this sample series, the sample label is formed by its batch label followed by underscore and a letter from 'a' to 'f'.

The DLC film thicknesses were found as follows: 10 nm for batch 10_nm, 21 nm for batch 21_nm, 54 nm for batch 54_nm, 100 nm for batches100_nm_I and 100_nm_II, 120 nm for batch 120_nm, 178 nm for batch 178_nm, 380 nm for batch 380_nm, and 570 nm for batch 570_nm.

Patterned back-etching was performed on DLC/Cu samples from the abovementioned series, also after the frame unmounting. In principle, this fabrication stage was the same as in the case of the sample series from the Chapter 4 (unpolished substrates), the difference consisting of durations involved and of the redoing of the spraying and thermal curing if needed [16] [17].

The labeling of the mask holes, substrate holes, and freestanding zones was also maintained.

Characterization by optical microscopy on the Cu side was made on samples after acetone rinse (photoresist removal) [17]. After the etching process of the substrate, the DLC film has become visible on fully corroded (empty) holes being in freestanding form. The average size of each full-corroded hole (average of the size values measured on that hole) was also measured [16]. Regarding the morphology, on DLC freestanding surface toward the substrate, the striations like those on the unpolished copper are missing, the striations-less morphology of polished Cu substrate being transferred onto DLC film at the interface to substrate.

The size of the freestanding zone of DLC film is identical to those of the corresponding hole on the back-etched Cu substrate.

The statistics of average sizes were obtained by Excel (the minimum of 667 µm, maximum of 2318 µm, mean of 1138 µm, STD of 402 µm, and STD to mean ratio of 35%).

The mean size of all achieved freestanding zones was close to the value of the diameter of UV mask holes (1 mm).

The optical microscopy at 50X magnification on the Cu side of freestanding zones reveals that the substrate morphology was transferred to the DLC film. The previously striations on the unpolished substrates are missed. The impurities/traces are present, having as possible sources the photoresist film, the incomplete corrosion leading to the micrometrical defects which consist of the remaining Cu material on DLC bottom surface, and the $FeCl_3$ solution bath. Generally, the flat zones lie on the areas of $5\times10^2 \div 5\times10^4$ µm^2, this means the well-focused surface zones in the images.

The rates of Cu holes completely etched, the rates of DLC freestanding zones survived, and the combined rates (the combination of these two rates by multiplication), until the optical microscopy investigation which was performed at maximum one day since the corrosion of substrate. The combined rate for groups of samples (batches) and for all samples (global) were found 15% for 54_nm, 93% for 380_nm, 58% for 570_nm, and 63% globally.

Optical profilometry tool was used to acquire, to untilt 3D profilograms and to determine S_q roughness of freestanding-film on bottom surface (Cu-side) and on top

surface (DLC-side), and of non-freestanding film, after photoresist removal, in confocal mode on 116.96×88.06 μm^2 scan area. HPL incidence occurs on the bottom surface, thus being the front side of target.

The statistics of 3D roughness (S_q) from profilograms acquired on bottom and top surfaces of (non-)freestanding DLC film was performed. The average, the STD, and the ratio of STD to average were calculated for DLC freestanding zones and for DLC non-freestanding. For 54_nm batch, on bottom surface, were found $S_{q(average)}$=0.9 μm, *STD*=0.6 μm and STD/$S_{q(average)}$=71.9%, on top surface, $S_{q(average\}}$=0.8 μm, *STD*=0.5 μm and STD/$S_{q(average)}$=58.9%, and on non-freestanding zone, $S_{q(average)}$=48 nm, *STD*=28 nm and STD/$S_{q(average)}$=58%. On the large region, the 3D-roughness for freestanding zone exceeds the *λ/10* limit but for non-freestanding zone is under the limit. Therefore, the DLC film itself meets this requirement on polished Cu substrate even at large scale, and the exceeding on freestanding zone only occurs at large region, but not at smaller scale (comparable with the HPL focus spot sizes) as will be shown later.

Gwyddion data processing of 3D profilograms acquired on bottom surface of freestanding DLC film was used to check if the surface has the roughness in limit of *λ/10*≈81 nm. One freestanding zone for each batch was selected for this processing. For each selected zone, 12 line-profiles of length of ~30 μm and ~90÷110 μm were extracted from its raw (tilted) 3D profilogram [16] [17]. These raw line-profiles were software processed to untilt by subtraction with fit line, following 2D roughness (R_q) calculus.

The R_q average by batch and globally were found 79 nm for 54_nm, 73 nm for 380_nm, and 76 nm globally. Percentages of 67%÷75% from the measured values are lower or equal to the *λ/10*=81 nm limit, where *λ*=810 nm for ELI-NP HPL system, being the roughness upper limit on zones with sizes which cover diameters domain of all used HPL focus spots (theoretical minimum diameter of focus spot is *1.2·λ*≈1 μm for this wavelength) [16]. The R_q average global (76 nm) is lower than the same *λ/10* limit. The missing substrate scratches (striations) explain these enhanced R_q-roughness values. Because the substrate morphology is transferred to the bottom surface of freestanding DLC, the substrate polishing has removed striations and has decreased R_q roughness below the *λ/10* limit on most profiles on the bottom surface of the freestanding film.

The EDX was used for the bottom [16] [17] and top surfaces of the freestanding DLC film of holes from a sample of 380 nm thickness (chemical elemental analysis). It is important to note the etchant of substrate is not in contact with the top DLC surface due to the photoresist isolation, but with the bottom surface since the substrate is removed at the interface to the DLC film. The Fe and Cu bottom traces are in small quantities acceptable for acceleration involving TNSA mechanism where the ion/proton fluxes provide from top surface layer (including C_xH_y and H_2O adsorbed air traces) [16] [18] which is very clean regarding these elements. The bottom surface and middle layers provide hot electrons which pass through film toward the top surface and exit from it triggering acceleration by charge separation [9] [20], not providing a Fe/Cu ion flow as HPL experiment in which DLC film was used shows [16] (Figure 5.3). So, it is less important from which atomic species these electrons come. Instead, this low importance level is less and less applicable with decreasing thickness, for TNSA regime, the solution to increase purity consisting of many final rinse cycles of DLC/Cu samples with extreme

caution to avoid breaking the freestanding areas. There is indicated to maintain an equilibrium between survival rate and final rinse clean, considering the TNSA occurring conditions and film thickness.

Toward simple target ensemble fabrication (Figure 5.1), the cutting and fixing the DLC/Cu samples were performed [16], obtaining the structure sketched in the Figure 5.2 shown below [17].

The availability of maximum four freestanding zones of one DLC/Cu sample is also applicable for this ensemble.

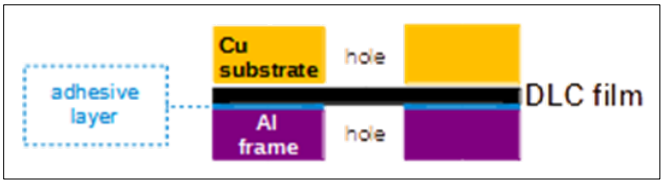

Figure 5.2: *Sketch for simple target ensemble*

Simple target ensembles were fabricated toward using in the commissioning campaign of experimental area E5 of ELI-NP from July-October 2021, to accelerate C and H ions from DLC films. These ensembles were constructed using DLC films with thicknesses of 380 nm and 570 nm, which have demonstrated their usability (not contaminating with adhesive at the mounting and not breaking) in more than half proportion after many days since assembling.

However, such targets still require careful manipulation until the mounting of the frame on the holder from the HPL interaction chamber to prevent DLC damage, but the survival rate should increase if this final mounting on the holder is made after as few days as possible since the end of target fabrication.

Two of these fabricated targets were used in the commissioning campaign within ELI-NP for the acceleration of C/H ions through the TNSA mechanism [16]. The acceleration experiment [47] has achieved the results shown in Figure 5.3 using a simple target ensemble with DLC film thickness of 380 nm. The energy of HPL pulse was E_{HPL}=19 J before the plasma mirror. The flows of the accelerated C ions and protons vs. kinetic energy are represented in the spectrum. The energy values from which the flows become undetectable (the cut-off energy) were ~180 MeV for carbon ions and ~38 MeV for protons.

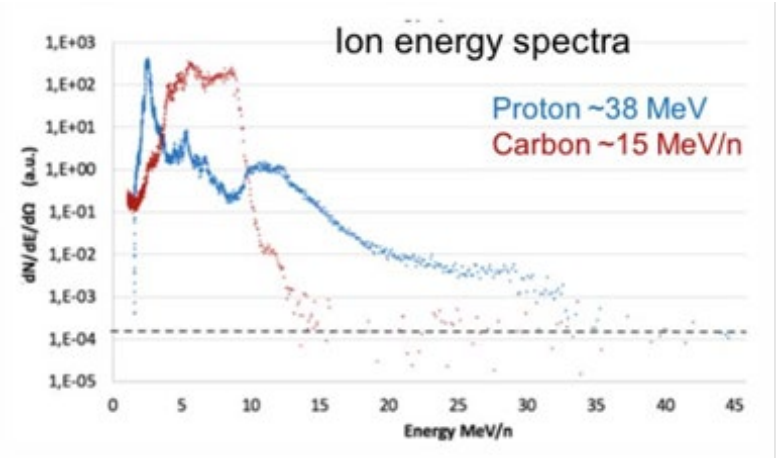

Figure 5.3: *Acceleration results in commissioning campaign for 380 nm DLC film; figure taken from the bibliographic reference* [47]

Chapter 6

Conclusions

The Cu substrate patterning which uses UV-lithography has an acceptable precision relative to the design of holes configuration, regarding the HPL targets applications. Freestanding DLC films are achieving in a proportion greater than half, considering entire patterning process. Freestanding DLC films survive after the entire patterning process, during optical microscopy and, without considerable losses, until optical profilometry.

Generally, the holes in the substrate are slightly larger on the Cu side than on the DLC side due to the isotropy of the chemical corrosion that removes the substrate material at the same etching rate in all directions. Never the hole size on the front side (Cu side) is smaller than on the DLC side, a situation which could have led to an unwanted incidence of HPL pulse on the substrate instead on target film during the interaction, the final alignment of the target in HPL focus being made by an optical tool from the rear side (DLC side), thus not being visible the front side.

The proportion of achieved freestanding DLC films is greater than half, considering the entire patterning process, and it is kept at least during optical microscopy. These survival rates reveal the importance of a more sp^3 C content in DLC film to enhance the mechanical behavior (higher tensile and shear strength) which sustains such achievement level. Last but not least, this chemical-mechanical linking is also reflected in the usability of at least half of target ensembles after a sufficient number of days since their mounting.

For most line-profiles on freestanding DLC film on the front side, the R_q roughness is lower or equal to the $\lambda/10$=81 nm limit. The S_q roughness of freestanding film (front side) on large areas is higher than this $\lambda/10$ limit, for DLC both on unpolished and polished substrates, because of film wrinkling on regions larger than the sizes of HPL focus spot. Thus, the wrinkling does not affect the use of films as targets in HPL experiments due to its presence on areas larger than the laser spots. The wrinkles can be generated by mechanical stress relief after the corrosion of Cu. This internal mechanical stress is caused

by the different thermal expansion of DLC than Cu, during the PECVD process in which the formed plasma heats both materials at a higher temperature than in the laboratory. Another explanation may be the deformation of freestanding film during the final rinsing of photoresist.

Considering the abovementioned, the freestanding DLC films produced during the research conducted for this thesis have demonstrated the potential to be used for HPL targets.

The research performed in this thesis has meet the proposed goal of developing optimized targets for the carbon ion and proton laser-driven acceleration, using low-resource manufacturing. This desiderate has requested high aspect ratio thin films with *λ/10* roughness limit on laser spot area and good mechanical strength, also attainable by an accessible fabrication chain in order to be on-site implementable within HPL emplacement.

The achieved results consist of fabrication methods, HPL targets, and ion acceleration measurements. The fabrication methods consist of a DLC deposition method by PECVD for growth thin films of tens and hundreds of nanometers including a substrate polishing method, an UV-lithography method for obtaining patterned freestanding films, and a method of mounting DLC film on target support. The targets consist of mono/bi-layer structures involving freestanding DLC films on corroded Cu substrates. The ion acceleration measurements consist of the energy spectra of carbon ions and protons.

The performed research contributes to the evolving of HPL field by providing a facile fabrication method of thin targets without micro/nanostructure for carbon ion and proton acceleration at near- and sub-petawatt pulse power.

The accessibility of the fabrication method is based on two facts. One is that the chemical route of freestanding patterning (substrate etching) confers accessibility to the method by using quite common reagents and laboratory tools. Second is that the roughness enhancement of the substrates by mechanical processing on a widely used polishing machine allows the using of raw materials with poor smoothness such as commercially available metallic sheets.

The PECVD process was optimized regarding the carbon-hydrogen stoichiometry of the precursor mixture, in order to obtain DLC thin films meeting the carbon hybridization ratios which the requirements of laser-driven acceleration experiments from ELI-NP involve.

The mounting method of the freestanding DLC/Cu structures on the frames to prepare the target ensembles for the experiments with high-power laser pulses performed within ELI-NP facility.

The list of original publications/works and of projects is shown below:

1) Published journal papers **(1st author)**:

- **L. Dincă**, C. Jalbă, B. Diaconescu, B. Mitu, ’Free-standing carbon targets for enhanced carbon ion acceleration with petawatt class lasers’, *U.P.B. Scientific Bulletin - Series A*, Vol. 85, Issue 4, 2023, ISSN 1223-7027, https://www.scientificbulletin.upb.ro/rev_docs_arhiva/rez1a1_218560.pdf;

- **L. Dincă**, C. Jalbă, B. Diaconescu, M. Cernăianu, P. Ghenuche, B. Mitu, T. Asavei, F. Rotaru, 'The challenges of using double targets as a novel contrast-enhancement method for laser-driven acceleration', *U.P.B. Scientific Bulletin - Series A*, Vol. 86, Issue 1, 2024, ISSN 1223-7027, https://www.scientificbulletin.upb.ro/rev_docs_arhiva/rez32b_567280.pdf.

2) Published journal papers **(co-author)**:

- A. Magureanu, **L. Dinca**, C. Jalba, R. F. Andrei, I. Burducea, D. G. Ghita, V. Nastasa, M. Gugiu, T. Asavei, O. Budriga, D. Ticos, V. Craciun, B. Diaconescu, C. M. Ticos, 'Target characteristics used in laser-plasma acceleration of protons based on the TNSA mechanism', *Frontiers in Physics*, *Sec. Interdisciplinary Physics*, Vol. 10, 2022, https://doi.org/10.3389/fphy.2022.727718;
- C. Jalbă, **L. Dincă**, N. Djourelov, C. Ticoș, A. Măgureanu, B. Diaconescu, 'The importance of chemical shift screening of the precursors for increasing the exfoliation efficiency of the graphite layers', *U.P.B. Scientific Bulletin - Series A*, Vol. 85, Issue 3, 2023, ISSN 1223-7027, https://www.scientificbulletin.upb.ro/rev_docs_arhiva/rez72e_153904.pdf.

3) Oral presentations **(1st author)**:

- **L. C. Dinca**, 'Carbonic thin films as targets for high-power laser beams', *ELI-NP Young Researchers' Competition 2018* (ELI-NP, Măgurele, Romania, November 28th-29th, 2018);
- **L. Dinca**, B. Diaconescu, V. Sătulu, V. Mărăscu, B. Mitu, C. Gheorghiu, 'Thin films for laser-driven acceleration of carbon ions', *SDIALA Educational Session 2018-2019* (Romania, Măgurele, April 18th 2019).

4) Poster presentations **(1st author)**:

- **L. Dinca**, B. Diaconescu, C. Gheorghiu, 'Characterization methods of ferrofluids usable in plasma mirror applications', *Nuclear Photonics 2018* (Brașov, Romania, June 24th-29th 2018);
- **L. Dinca**, B. Diaconescu, V. Satulu, V. Marascu, C. Gheorghiu, B. Mitu, 'Carbon-based thin films for high-power laser applications', *XVIIIth International Conference on Plasma Physics and Applications* (Iași, Romania, June 20th-22nd 2019);
- **L. Dinca**, B. Diaconescu, B. Mitu, V. Satulu, 'Fabrication and characterization methods of carbon thin films for high-power laser applications', *ELI-NP Summer School 2019* (Sinaia, Romania, September 9th-13th 2019);
- **L. Dinca**, C. Jalba, B. Diaconescu, B. Mitu, 'Free-standing carbon targets for commissioning experiments at ELI-NP', *International Conference on Laser,*

Plasma and Radiation – Science and Technology 2022 (Bucharest, Romania, June 7th-10th 2022).

5) ELI-NP activity reports:

- C. Gheorghiu, A. Ionescu, **L. Dinca**, A. Serban, V. Ene, I. Zai, D. Popa, V. Leca, 'The ELI-NP Target Laboratory, research program and preliminary targets', *ELI-NP RA3 Scientific & Technical Reports 2018-2019* (ELI-NP internal use only);
- Cernaianu M. O., Ghenuche P. V., Rotaru F., Asavei T., Balascuta S., Chalus O., Dancus I., Diaconescu C. B., **Dinca L.**, Dreghici D. B., Ghita D. G., Gugiu M. M., Jalba C., Lupu A. M., Magureanu A., Matei D. G., Nastasa V. V., Negoita F., Popescu D., Soderstrom P. A., Tataru M., Tanaka K. A., Ticos C. M., Tomassini P., Tudor L., Ur C. A., Doria D., 'Commissioning of the 1 PW experimental area with an experiment on TNSA ion acceleration', *ELI-NP Annual Report 2020-2021*, https://www.eli-np.ro/documents/ELI-NP-Annual_Report-2020-2021.pdf.

6) Project contract on which the Ph.D. student has worked:

- ELI-NP phase II, co-financed by the Romanian Government and the European Union through the European Regional Development Fund – the Competitiveness Operational Program (contract no. 1/07.07.2016, COP, ID 1334).

The fabrication chain developed within this research work present the interest for testing future extension to DLC freestanding patterns with larger areas suitable for plasma mirror applications. Such structures need lateral openings with diameters of at least 10 mm because of laser spot size at several centimeters before the focus point. An important issue for this case consists of the freestanding film wrinkling which leads to the deformation of the wavefront of incident HPL pulse and, consequently, of the focus spot shape with potential negative effects on the acceleration process [16], while the surface topography of the plasma mirror in the initial solid state are also taken over in the final plasma state between the pre-pulse and main pulse arrivals [48]. A viable proposal to solve this problem is the PECVD holder cooling to maintain on the substrate during on the exothermal DLC deposition process the ambient temperature from entire subsequent steps before the target laser-shooting. This procedure should prevent the inequal thermal deformations of the substrate and film during on the PECVD heating and cooling to the room temperature after the deposition step.

Other further development consists of the extension to other kinds of carbon-based films concerning on the same goals of this thesis and keeping the steps which involve Cu substrate processing. An important challenge of such further development is the achievement of freestanding ultra-thin films proper to engage the RPA mechanism to generate quasi-monoenergetic, bright and collimated high-energy carbon ion beams with 10 PW laser power available at ELI-NP. As a significant fact, these ion sources exhibit the potential to push forward the hadron therapy toward the energy per nucleon ratios

required for a high effectiveness of the tumoral tissue destruction in the oncological applications.

Bibliography

[1] M. Pessot, P. Maine and G. Mourou, "1000 times expansion/compression of optical pulses for chirped pulse amplification," *Optics Communications,* vol. 62, pp. 419-421, 1987.

[2] J. W. Yoon, C. Jeon, J. Shin, S. K. Lee, H. W. Lee, I. W. Choi, H. T. Kim, J. H. Sung and C. H. Nam, "Achieving the laser intensity of 5.5×10^{22} W/cm² with a wavefront-corrected multi-PW laser," *Opt. Express,* vol. 27, p. 20412–20420, July 2019.

[3] C. Scullion, D. Doria, L. Romagnani, A. Sgattoni, K. Naughton, D. R. Symes, P. McKenna, A. Macchi, M. Zepf, S. Kar and M. Borghesi, "Polarization dependence of bulk ion acceleration from ultrathin foils irradiated by high-intensity ultrashort laser pulses," *Phys. Rev. Lett.,* vol. 119, no. 5, p. 054801, August 2017.

[4] J. Badziak, "Laser-driven ion acceleration: Methods, challenges and prospects," *Journal of Physics: Conference Series,* vol. 959, p. 012001, January 2018.

[5] B. M. Hegelich, B. J. Albright, J. Cobble, K. Flippo, S. Letzring, M. Paffett, H. Ruhl, J. Schreiber, R. K. Schulze and J. C. Fernández, "Laser acceleration of quasi-monoenergetic MeV ion beams," *Nature,* vol. 439, p. 441–444, January 2006.

[6] S. S. Bulanov, C. B. Schroeder, E. Esarey and W. P. Leemans, "Optimized laser pulse profile for efficient radiation pressure acceleration of ions," *Physics of Plasmas,* vol. 19, p. 093112, 2012.

[7] A. Higginson, R. J. Gray, M. King, R. J. Dance, S. D. R. Williamson, N. M. H. Butler, R. Wilson, R. Capdessus, C. Armstrong, J. S. Green, S. J. Hawkes, P. Martin, W. Q. Wei, S. R. Mirfayzi, X. H. Yuan, S. Kar, M. Borghesi, R. J. Clarke, D. Neely and P. McKenna, "Near-100 MeV protons via a laser-driven transparency-enhanced hybrid acceleration scheme," *Nature Communications,* vol. 9, p. 724, February 2018.

[8] T. M. Ostermayr, C. Kreuzer, F. S. Englbrecht, J. Gebhard, J. Hartmann, A. Huebl, D. Haffa, P. Hilz, K. Parodi, J. Wenz, M. E. Donovan, G. Dyer, E. Gaul, J. Gordon, M. Martinez, E. Mccary, M. Spinks, G. Tiwari, B. M. Hegelich and J. Schreiber,

"Laser-driven X-ray and proton micro-source and application to simultaneous single-shot bi-modal radiographic imaging," *Nature Communications,* vol. 11, p. 6174, December 2020.

[9] A. Măgureanu, L. Dincă, C. Jalbă, R. F. Andrei, I. Burducea, D. G. Ghiţă, V. Nastasa, M. Gugiu, T. Asavei, O. Budrigă, D. Ticoş, V. Crăciun, B. Diaconescu and C. M. Ticoş, "Target characteristics used in laser-plasma acceleration of protons based on the TNSA mechanism," *Frontiers in Physics, Sec. Interdisciplinary Physics,* vol. 10, 2022.

[10] G. Milluzzo, H. Ahmed, L. Romagnani, D. Doria, P. Chaudhary, C. Maiorino, A. McIlvenny, A. McMurray, K. Polin, Y. Katzir, R. Pattathil, P. McKenna, K. Prise and M. Borghesi, "Dosimetry of laser-accelerated carbon ions for cell irradiation at ultra-high dose rate," *Journal of Physics: Conference Series,* vol. 1596, p. 012038, July 2020.

[11] D. Schardt, "Tumor therapy with high-energy carbon ion beams," *Nuclear Physics A,* vol. 787, pp. 633-641, 2007.

[12] A. Maksimchuk, S. S. Bulanov, A. Brantov, V. Y. Bychenkov, V. Chvykov, F. Dollar, D. Litzenberg, G. Kalintchenko, T. Matsuoka, S. Reed, V. Yanovsky and K. Krushelnick, "Control of proton energy in ultra-high intensity laser-matter interaction," *Journal of Physics: Conference Series,* vol. 244, p. 042025, August 2010.

[13] F. T. Thema, P. Beukes, B. D. Ngom, E. Manikandan and M. Maaza, "Free standing diamond-like carbon thin films by PLD for laser based electrons/protons acceleration," *Journal of Alloys and Compounds,* vol. 648, pp. 326-331, 2015.

[14] B. M. Hegelich, I. Pomerantz, L. Yin, H. C. Wu, D. Jung, B. J. Albright, D. C. Gautier, S. Letzring, S. Palaniyappan, R. Shah, K. Allinger, R. Hörlein, J. Schreiber, D. Habs, J. Blakeney, G. Dyer, L. Fuller, E. Gaul, E. Mccary, A. R. Meadows, C. Wang, T. Ditmire and J. C. Fernandez, "Laser-driven ion acceleration from relativistically transparent nanotargets," *New Journal of Physics,* vol. 15, p. 085015, August 2013.

[15] M. O. Cernăianu, P. V. Ghenuche, F. Rotaru, T. Asavei, S. Bălăşcuţă, O. Chalus, I. Dancus, C. B. Diaconescu, L. Dinca, D. B. Dreghici, D. G. Ghiţă, M. M. Gugiu, C. Jalba, A. M. Lupu, A. Măgureanu, D. G. Matei, V. V. Nastasa, F. Negoita, D. Popescu, P. A. Söderström, M. Tataru, K. A. Tanaka, C. M. Ticoş, P. Tomassini, L. Tudor, C. A. Ur and D. Doria, "Commissioning of the 1 PW experimental area with an experiment on TNSA ion acceleration," *ELI-NP Annual Report 2020-2021,* p. 91, June 2022, ELI-NP.

[16] L. Dinca, C. Jalba, B. Diaconescu and B. Mitu, "Free-standing carbon targets for enhanced carbon ion acceleration with Petawatt class lasers," *U.P.B. Scientific Bulletin - Series A,* vol. 85, pp. 171-178, 2023.

[17] L. Dinca, C. Jalba, B. Diaconescu and B. Mitu, "Free-standing carbon targets for commissioning experiments at ELI-NP," *International Conference on Laser, Plasma and Radiation – Science and Technology 2022*, Bucharest, Romania, June 7-10, 2022.

[18] L. Dincă, C. Jalbă, B. Diaconescu, M. Cernăianu, P. Ghenuche, B. Mitu, T. Asavei and F. Rotaru, "The challenges of using double targets as a novel contrast-enhancement method for laser-driven acceleration," *U.P.B. Scientific Bulletin - Series A,* vol. 86, 2024.

[19] J. Park, S. S. Bulanov, J. Bin, Q. Ji, S. Steinke, J.-L. Vay, C. G. R. Geddes, C. B. Schroeder, W. P. Leemans, T. Schenkel and E. Esarey, "Ion acceleration in laser generated Megatesla magnetic vortex," *Physics of Plasmas,* vol. 26, p. 103108, 2019.

[20] D. Sangwan, O. Culfa, C. P. Ridgers, S. Aogaki, D. Stutman and B. Diaconescu, "Simulations of carbon ion acceleration by 10 PW laser pulses on ELI-NP," *Laser and Particle Beams,* vol. 37, p. 346–353, 2019.

[21] K. P. Furlan, A. N. Klein and D. Hotza, "Diamond-like carbon films deposited by hydrocarbon plasma sources," *Reviews on Advanced Materials Science,* vol. 34, pp. 165-172, 2013.

[22] L. Dinca, B. Diaconescu, V. Sătulu, V. Mărăscu, B. Mitu and C. Gheorghiu, "Thin films for laser-driven acceleration of carbon ions," *SDIALA Educational Session 2018-2019*, Romania, Măgurele, April 18, 2019.

[23] L. C. Dinca, "Carbonic thin films as targets for high-power laser beams," *ELI-NP Young Researchers' Competition 2018*, ELI-NP, Măgurele, Romania, November 28-29, 2018.

[24] H. O. Pierson, "Handbook of carbon, graphite, diamonds and fullerenes - Processing, properties and applications," Ed. William Andrew Publishing, Oxford, 1994, ISBN 978-0-8155-1339-1.

[25] M. C. Salvadori, D. R. Martins and M. Cattani, "DLC coating roughness as a function of film thickness," *Surface and Coatings Technology,* vol. 200, pp. 5119-5122, 2006.

[26] F. Garrelie, A. S. Loir, F. Goutaland, C. Donnet, R. L. Harzic, B. Angleraud, Y. Ouerdane and P. Laporte, "Diamond-like carbon deposited by femtosecond pulsed-laser ablation: Evidence of nanocrystalline diamond," in *High-Power Laser Ablation IV*, 2002.

[27] Y. Jeon, Y. S. Park, H. J. Kim, B. Hong and W. S. Choi, "Tribological properties of ultrathin DLC films with and without metal interlayers," *Journal of Korean Physical Society,* vol. 51, p. 1124–1128, September 2007.

[28] L. Dinca, B. Diaconescu, B. Mitu and V. Satulu, "Fabrication and characterization methods of carbon thin films for high-power laser applications," *ELI-NP Summer School 2019*, Sinaia, Romania, September 9-13, 2019.

[29] L. Dinca, B. Diaconescu, V. Satulu, V. Marascu, C. Gheorghiu and B. Mitu, "Carbon-based thin films for high-power laser applications," *XVIIIth International Conference on Plasma Physics and Applications*, Iași, Romania, June 20-22, 2019.

[30] N. Pinel, C. Bourlier and J. Saillard, "Degree of roughness of rough layers: Extensions of the Rayleigh roughness criterion and some applications," *Progress In Electromagnetics Research B,* vol. 19, pp. 41-63, 2010.

[31] F. Ulaby, D. Long, W. Blackwell, C. Elachi, A. Fung, C. Ruf, K. Sarabandi, J. Zyl and H. Zebker, "Microwave radar and radiometric remote sensing," Chapter 10: "Surface scattering models and land observations," 2014, ISBN: 978-0-472-11935-6.

[32] M. Hiratsuka, H. Nakamori, K. O. G. O. Yasuo, M. Sakurai, N. Ohtake and H. Saitoh, "Correlation between optical properties and hardness of diamond-like carbon films," *Journal of Solid Mechanics and Materials Engineering,* vol. 7, pp. 187-198, 2013.

[33] M. Cernaianu, "Laser produced plasma optics," *ELI-NP Summer School 2019 - Nuclear Physics with High Power Lasers (September 9-13, 2019, Sinaia, Romania)*.

[34] G. Doumy, F. Quéré, O. Gobert, M. Perdrix, P. Martin, P. Audebert, J. C. Gauthier, J.-P. Geindre and T. Wittmann, "Complete characterization of a plasma mirror for the production of high-contrast ultraintense laser pulses," *Phys. Rev. E,* vol. 69, no. 2, p. 026402, February 2004.

[35] D. Ursescu, D. Matei, M. Talposi, V. Iancu, V. Aleksandrov, G. Bleotu, A. Naziru, O. Tesileanu, M. Rosu, Y. Nakamiya, M. O. Cernaianu, B. de Boisdeffre, C. Ene, M. Caragea, A. Lazar, M. Kiss, M. Masruri, L. Caratas, A. Toader, D. Nistor, V. Luta, B. Tatulea, D. Popa, N. Stan, T. Jitsuno, R. Banici, A. Baleanu, A. Gradinariu, J. Wheeler, G. Mourou and I. Dancus, "First HPLS experiments at ELI-NP: Spectral broadening in thin films," *ELI-NP Annual Report 2020-2021,* p. 33, June 2022, ELI-NP.

[36] D. Doria, P. V. Ghenuche, M. O. Cernăianu, P. Tomassini, A. Berceanu, J. F. Ong, N. Safca, A. Măgureanu, M. Talposi, M. Matei, L. Tudor, S. Bălăşcuţă, M. M. Gugiu, M. Cuciuc, I. Dancus, C. B. Diaconescu, I. O. Mitu, V. V. Nastasa, F. Negoita, V. R. M. Rodrigues, M. M. Rosu, D. Stutman, K. A. Tanaka, C. A. Ur, D. Ursescu, N. V. Zamfir and C. M. Ticoş, "First experiment with a laser-focused beam at ELI-NP: Laser-driven electron acceleration with the 100 TW laser system," *ELI-NP Annual Report 2020-2021,* p. 87, June 2022, ELI-NP.

[37] C. Gheorghiu, A. Ionescu, L. Dinca, A. Serban, V. Ene, I. Zai, D. Popa and V. Leca, "The ELI-NP Target Laboratory, research program and preliminary targets," *Scientific & Technical Reports 2018/2019,* Vols. Research Activities 3 - Nuclear

Physics with High Power Lasers, Part II: Biomedical & Target Laboratory, p. 23–28, 5 July 2019, ELI-NP (ELI-NP internal use only).

[38] K. E. Spear, "Chemical and energetic aspects of CVD diamond growth," *Preprints of Papers, American Chemical Society, Division of Fuel Chemistry; USA,* vol. 34:2, January 1989.

[39] J. J. Gracio, Q. H. Fan and J. C. Madaleno, "Diamond growth by chemical vapour deposition," *Journal of Physics D: Applied Physics,* vol. 43, p. 374017, September 2010.

[40] P. S. Banks, L. Dinh, B. C. Stuart, M. D. Feit, A. M. Komashko, A. M. Rubenchik, M. D. Perry and W. McLean, "Short-pulse laser deposition of diamond-like carbon thin films," *Applied Physics A,* vol. 69, p. S347–S353, December 1999.

[41] A. Henig, D. Kiefer, K. Markey, D. C. Gautier, K. A. Flippo, S. Letzring, R. P. Johnson, T. Shimada, L. Yin, B. J. Albright, K. J. Bowers, J. C. Fernández, S. G. Rykovanov, H.-C. Wu, M. Zepf, D. Jung, V. K. Liechtenstein, J. Schreiber, D. Habs and B. M. Hegelich, "Enhanced laser-driven ion acceleration in the relativistic transparency regime," *Phys. Rev. Lett.,* vol. 103, no. 4, p. 045002, July 2009.

[42] P. K. Bachmann, D. Leers and H. Lydtin, "Towards a general concept of diamond chemical vapour deposition," *Diamond and Related Materials,* vol. 1, pp. 1-12, August 1991.

[43] P. K. Bachmann and W. van Enckevort, "Diamond deposition technologies," *Diamond and Related Materials,* vol. 1, pp. 1021-1034, 1992.

[44] J. Díaz, G. Paolicelli, S. Ferrer and F. Comin, "Separation of the sp^3 and sp^2 components in the C1s photoemission spectra of amorphous carbon films," *Phys. Rev. B,* vol. 54, no. 11, p. 8064–8069, September 1996.

[45] C. Jalbă, L. Dincă, N. Djourelov, C. Ticoș, A. Măgureanu and B. Diaconescu, "The importance of chemical shift screening of the precursors for increasing the exfoliation efficiency of the graphite layers," *U.P.B. Scientific Bulletin - Series A,* vol. 85, 2023.

[46] H. Jansen, H. Gardeniers, M. de Boer, M. Elwenspoek and J. Fluitman, "A survey on the reactive ion etching of silicon in microtechnology," *J. Micromech. Microeng.,* vol. 6, p. 14–28, 1996.

[47] webpage "E5 experimental room," ELI-NP, https://users.eli-np.ro/e5.php.

[48] L. Dinca, B. Diaconescu and C. Gheorghiu, "Characterization methods of ferrofluids usable in plasma mirror applications," *Nuclear Photonics 2018*, Brașov, Romania, June 24-29, 2018.